(Received 20 November 2023, Accepted 3 February 2024, Scheduled 15 February 2024)

Dual-Band Implantable Antenna Loaded with Patch Slots for Wireless Biotelemetry Systems

Md. Masud Rana[1,*], Md. Ariful Islam[1], and Ibrahim M. Mehedi[2]

[1] *Department of Electrical and Electronic Engineering, Rajshahi University of Engineering and Technology Rajshahi 6204, Bangladesh*
[2] *Department of Electrical and Computer Engineering, King Abdulaziz University, Jeddah, Saudi Arabia*

ABSTRACT: This paper presents a dual-band implantable antenna with coaxial probe feeding for wireless biotelemetry applications. The antenna features spiral patches, resulting in a compact size of $27 \times 14 \times 1.6\,\text{mm}^3$. It can operate in two different frequency bands, 241–641 MHz and 1.17–2.06 GHz, providing coverage for the medical implant communication service (MICS) band and the industrial, scientific, and medical (ISM) band. This simple design offers improved return loss and higher bandwidths that are achieved by incorporating patch slots and shortening pins in spiral patches, representing a significant contribution to the field of dual-band antenna design for wireless biotelemetry systems. In the human body phantom model, the SAR values of 48.9 mW/kg and 1.19 W/kg are achieved, which satisfy the IEEE standard safety constraints. An experimental prototype of the proposed antenna is fabricated, demonstrating acceptable return loss and VSWR.

1. INTRODUCTION

The smart things in our environment are now wirelessly connected in the new Internet of Things (IoT) age. The wireless body area networks (WBANs) and biotelemetry capabilities are becoming crucial to the integration of the IoT ecosystem [1]. Wireless biomedical systems are developed to observe, diagnose, treat, and wirelessly transmit physiological data from patients [2–5]. Wireless biotelemetry, in particular, enables the minimally invasive monitoring of physiological parameters, leading to enhanced patient comfort and care and substantially reducing hospital expenditures [6]. Current advancements in these systems have enabled the investigation of heart rate [7] and glucose level monitoring [8], as well as facilitating measurements for body temperature, intracranial pressure [9, 10], capsule endoscopies [11, 12], retinal prostheses [13], and cardiac pacemakers [2]. In the literature, numerous approaches exist for developing antennas for wireless biotelemetry systems. Among them is the use of slots in radiators [14], spiral patches [15], circular patches [16], defective ground structures [17], and fractal structures [18]. A differentially fed dual-band antenna can be used for a fully implantable neuro-microsystem [19]. It allows high-data-rate implanted brain recording devices by enabling sub-GHz wideband transmission. Later, the spiral and serpentine-shaped antennas are also utilized for operating in the MICS band [20]. The finite difference time domain (FDTD) method can be implemented to assess important antenna parameters and compare the findings to measurements. Again, radio frequency identification (RFID) based antenna can be used in wireless biotelemetry systems [21]. A planar inverted-F antenna (PIFA) structured antenna can serve the biotelemetry applications. A PIFA-structured antenna is developed for triple-band applications [22]. The model of this antenna has four layers. The radiating components of the antenna are located in layers 1, 2, 3, and 4, with layer 1 serving as the ground plane. A coplanar waveguide (CPW) fed ultra-miniaturized patch antenna along with slots in the ground plane can be utilized for wireless applications [23]. With the use of an umbrella-shaped metallic ground plane (UsMGP) and an improved radiator, a compact broadband and radiation efficient antenna can be developed [24]. A wideband ultra-compact implanted antenna (WUCIA) for biomedical applications is proposed in [25]. The WUCIA comprises a partial ground and a meandering radiator patch with variously shaped slots. The ultra-compact dimensions, low power loss, and compliance with safety norms of this antenna are its key accomplishments. An antenna based on a stacked PIFA structure, which includes a slot embedded in each radiating patch, is introduced in [26]. Again, an L-shaped transmission line fed anti-spiral resonator structure can be used for dual-band operation [27]. An H-shaped cavity slot antenna is proposed for short-range implantable devices in [28]. It is designed to operate in the ISM band and is investigated using the FDTD method. Ultra-wideband antennas with stable impedance matching are used to mitigate detuning effects for multiple wireless biotelemetric applications. Such antennas can be designed with two-sectioned spiral-shaped radiating patch and a slotted ground [29]. For an implantable antenna, it is important to mitigate the effects on human tissue. A thin film layer can be coated around the antenna to isolate the effect on human tissues and alleviate the

* Corresponding author: Md. Masud Rana (md.masud.rana.ruet@gmail.com).

TABLE 1. Optimized parameters of the proposed antenna.

Parameter	Value (mm)	Parameter	Value (mm)
l	13.5	h	0.9
b	14	i	0.4
c	1.5	j	0.5
d	0.8	k	0.3
e	1.2	m	1.6
f	1	n	0.035
g	0.5	p	4.8

electromagnetic coupling with the human body [30]. Multiple-input multiple-output (MIMO) antennas are also reported for biotelemetry applications. For example, a CPW-fed 3D MIMO ground radiating cubic antenna, implantable in the human upper arm for biotelemetry applications, is presented in [31]. Arteriovenous grafts (AVGs) represent essential, life-preserving implants utilized in the care of chronic kidney disease (CKD) patients undergoing hemodialysis (HD). A compact dual-band implantable antenna for HD monitoring is proposed in [32]. A circularly polarized antenna can be miniatured by etching C-shaped open slots on the patch [33]. A rectangular slot truncated diagonally is cut to improve the circular polarization performance of the antenna suggested in [34]. A multilayer circularly polarized helical antenna is demonstrated for ISM ingestible capsule endoscope systems in [35]. The size of the antennas that are designed for operating in the MICS band can be reduced by employing a meandering and shorting strategy [24]. This antenna is composed of three open loops at various layers connected via holes to form an axial-mode helical structure to generate travelling wave radiation. Dual-band coverage, higher return loss, and higher electrical length are the most advantageous characteristics of such antennas. Again, for brain implantable antennas, tiny and tuneable antennas can be designed using coupled split rings [36].

Proposed antenna based RFID tags are developed as the proof of this concept. A compact differential dual-frequency antenna with a stacked configuration is described in [37]. Contrasted with the traditional stacked dual-frequency antenna design, this model employs a radiating element spanning half a guided wavelength, distributed across two layers, and interconnected via holes, effectively reducing the antenna's overall dimensions. Most of these reported antennas have complex structures that are either difficult to fabricate or inappropriate for contemporary wireless devices. Though the described structures are able to achieve the permitted values for the antenna parameters, these values can still be improved.

This paper proposes an antenna that effectively operates in two bands (MICS band and ISM band). The proposed antenna is based on merging two spiral patches together on an FR-4 substrate and feeding any of the two patches individually. Patch slots are used to improve the return losses and enhance the bandwidths. Also, shortening pins are used to tune the resonant frequencies.

2. ANTENNA DESIGN METHODOLOGY

2.1. Geometry of the Proposed Antenna

Figure 1(a) shows the geometry of the proposed antenna. There are two spiral components in it. Each antenna element is $13.5 \times 14\,\text{mm}^2$ in size, and they are all symmetrically aligned having a total size of $27 \times 14\,\text{mm}^2$. The technique of coaxial probe feeding is used to feed each antenna element. By exciting any of the feedings, the antenna allows dual-band operation in the MICS band and near the ISM band, i.e., the two ports do not need to be excited simultaneously. The developed antenna is mounted on a 1.6 mm FR-4 substrate with a relative permittivity ε_{r} of 4.4 and a loss tangent of 0.025. The same material is used as a superstrate. This superstrate layer serves dual purposes: safeguarding the antenna against direct contact with the semiconducting tissue and serving as a buffer between the metal radiator and human tissues [17].

Moreover, a parametric investigation is conducted to assess the geometrical parameters' effects on the proposed antenna's performance and determine the optimum values of those parameters. The integration of patch slots within each antenna element plays a pivotal role in improving return losses and broadening bandwidths.

Again, incorporating shortening pins facilitates the fine-tuning of resonant frequencies, ensuring precise alignment with the desired operational bands. The detailed depiction of a single element comprising the proposed antenna and parameter dimensions are illustrated in Figures 1(b), (c), providing a clear insight into the antenna's physical structure and layout. Furthermore, the optimized parameter values crucial for the optimal functioning of the proposed antenna are outlined in Table 1.

2.2. Parametric Investigation

The effects of several geometrical parameters on resonant frequencies, bandwidth, and impedance matching properties are analyzed in this section through a detailed parametric investigation. Substrate height, substrate length, outer and inner spiral arm widths, etc., are the factors that influence the antenna performance parameters.

The simulated return loss S_{11} with varied substrate height (SH) is shown in Figure 2(a). The increase in the height SH decreases the second bandwidth as well as the return loss S_{11}. It can be demonstrated that $SH = 1.6\,\text{mm}$ can provide improved S_{11} value. Figure 2(b) depicts the effect of substrate length (SL)

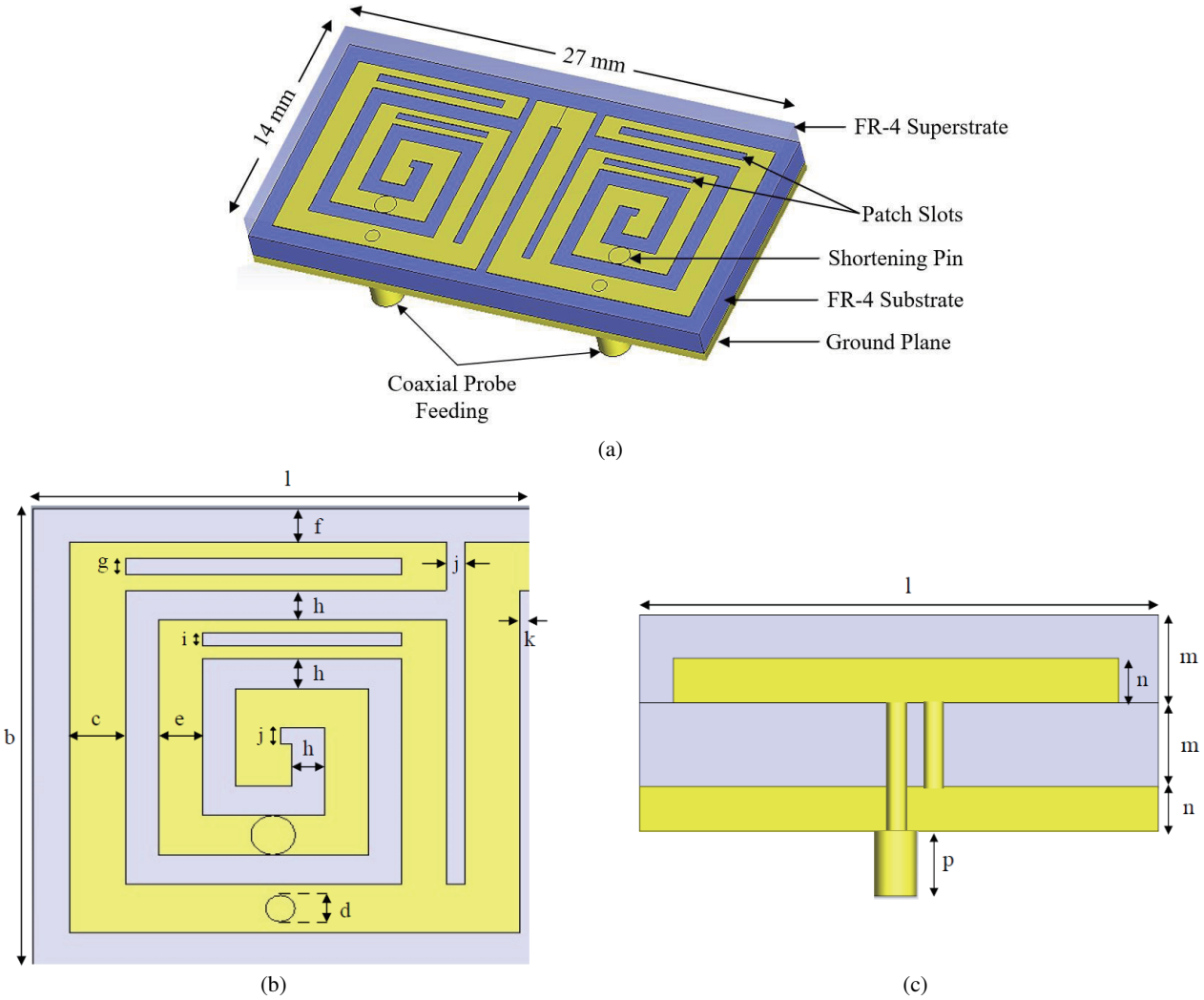

FIGURE 1. Proposed antenna geometry. (a) 3D view, (b) front view, and (c) side view.

on the S_{11}. An increment in SL reduces the operating frequency heavily. For $SL = 27$ mm, the second operating frequency is near 1.68 GHz whereas the first operating frequency is very close to the MICS band. So, the value of SL is taken as 27 mm to obtain greater performances in terms of resonant frequency. Figure 2(c) illustrates the simulated S_{11} with several values of the width of the outer spiral arm ($W1$). It does not affect the operating frequencies much, but it severely affects the magnitude of the return loss. It can be claimed from the figure that the value $W1 = 1.5$ mm exhibits the best performances in terms of impedance matching. The effect of the width of the inner spiral arm (W) is shown in Figure 2(d). It does not affect the operating frequencies much, but it severely affects the magnitude of the return losses at both frequencies. Furthermore, it can be noticed from the figure that the value $W = 1.2$ mm provides a good impedance matching at the operating frequencies.

After the analysis, the optimized set of values for the parameters are $SH = 1.6$ mm, $SL = 27$ mm, $W1 = 1.5$ mm, and $W = 1.2$ mm.

In Figure 3, the radiation pattern for $SH = 1.2$ mm is depicted, illustrating the values of gain and directivity in decibels. Similarly, the radiation pattern for various values of SH and other parameters (SL, $W1$, and W) are observed. The resulting gain and directivity values are detailed in Table 2. Efficiency values are computed by dividing the gain by the respective directivity values.

According to the results shown in Table 2, it is seen that the maximum efficiency is obtained for $SH = 1.6$ mm, $SL = 27$ mm, $W1 = 1.5$ mm, and $W = 1.2$ mm. Hence, this set of parameters can be selected as the optimized parameters.

3. RESULTS AND DISCUSSION

3.1. Numerical and Experimental Results

Initially, a single tissue layer is used as the simulation environment, followed by assessing the antenna's robustness within a three-layer (skin layer, fat layer, and muscle layer) tissue model. The simplified environment of the single-layer tissue is illustrated in Figure 4.

The structure of the proposed dual-band antenna is manufactured, and the S_{11} and voltage standing wave ratio (VSWR)

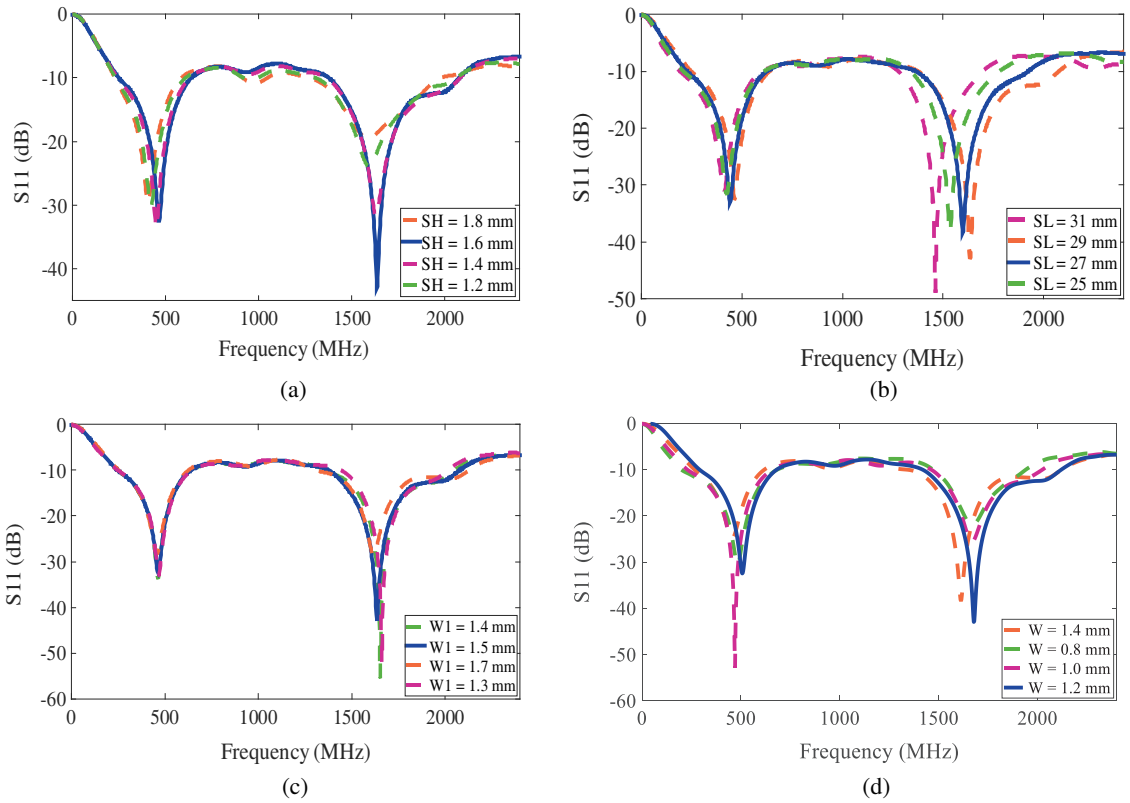

FIGURE 2. The effects of (a) substrate height (SH), (b) substrate length (SL), outer spiral patch width ($W1$), and inner spiral patch width (W) on the return loss S_{11} of the proposed antenna.

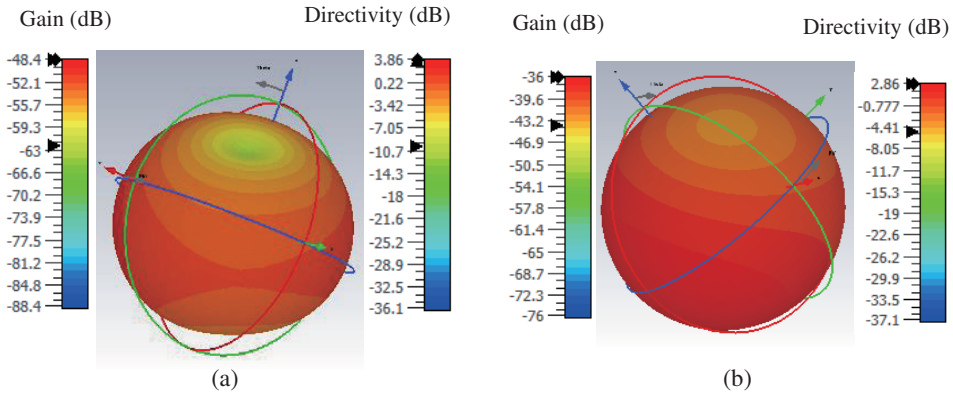

FIGURE 3. Gain and directivity for $SH = 1.2$ mm at (a) 467 MHz, and (b) 1.69 GHz.

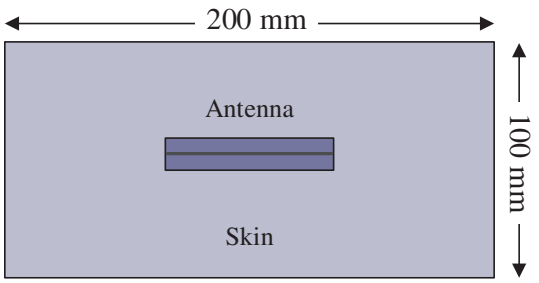

FIGURE 4. Simplified geometries for the one-layer tissue model.

TABLE 2. Gain, directivity and efficiency for different parameters.

Parameter	Value (mm)	Gain (dB)	Directivity (dB)	Efficiency (dB)
SH	1.2	−46.65	3.36	−13.88
		−18.30	6.86	−2.67
	1.4	−48.38	3.12	−15.50
		−18.93	6.15	−3.07
	1.6	−47.72	3.61	−13.21
		−17.72	6.54	−2.70
	1.8	−47.16	3.70	−12.74
		−17.79	6.73	−2.64
SL	31	−47.13	3.19	−14.77
		−17.9	6.76	−2.64
	29	−47.28	3.18	−14.86
		−18.11	6.75	−2.68
	27	−47.21	3.59	−13.15
		−18.07	6.54	−2.76
	25	−47.16	3.68	−12.81
		−17.85	6.53	−2.73
W1	1.4	−46.62	3.83	−12.17
		−18.11	6.16	−2.93
	1.5	−47.16	3.12	−15.11
		−17.85	6.18	−2.88
	1.7	−46.94	3.64	−12.89
		−17.96	6.44	−2.78
	1.3	−46.79	3.77	−12.14
		−17.57	6.73	−2.61
W	1.4	−46.62	3.39	−13.75
		−18.34	6.76	−2.71
	1.2	−47.16	3.38	−13.95
		−18.14	6.74	−2.69
	1.0	−46.94	3.59	−13.07
		−17.87	6.58	−2.71
	0.8	−46.79	3.18	−14.71
		−17.67	6.13	−2.89

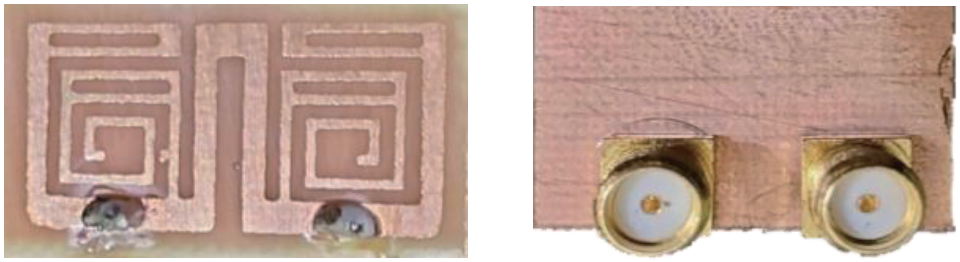

(a) (b)

FIGURE 5. (a) Front and (b) back view of the fabricated antenna.

are measured in free space using NanoVNA-V2. Due to the unavailability of pure FR-4 material, glass fiber is used as the substrate. Figures 5(a) and (b) represent the structure of the fabricated antenna, and Figure 6 illustrates the experimental setup for the measurement of the performance parameters of the manufactured antenna.

3.1.1. Return Loss (S11 Parameter) and VSWR

Figures 7(a) and (b) illustrate the variations of the return loss S_{11} and VSWR acquired by simulation and measurement versus frequency. According to the simulation results, the obtained return losses are −29.15 dB and −36.67 dB at the resonant frequencies of 444 MHz and 1.65 GHz, respectively. The first op-

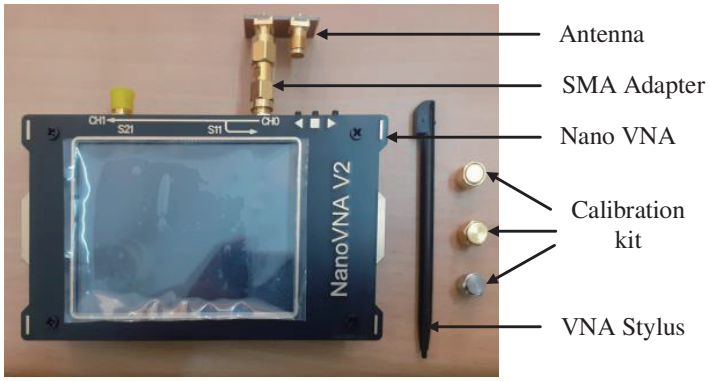

FIGURE 6. Setup for measurement.

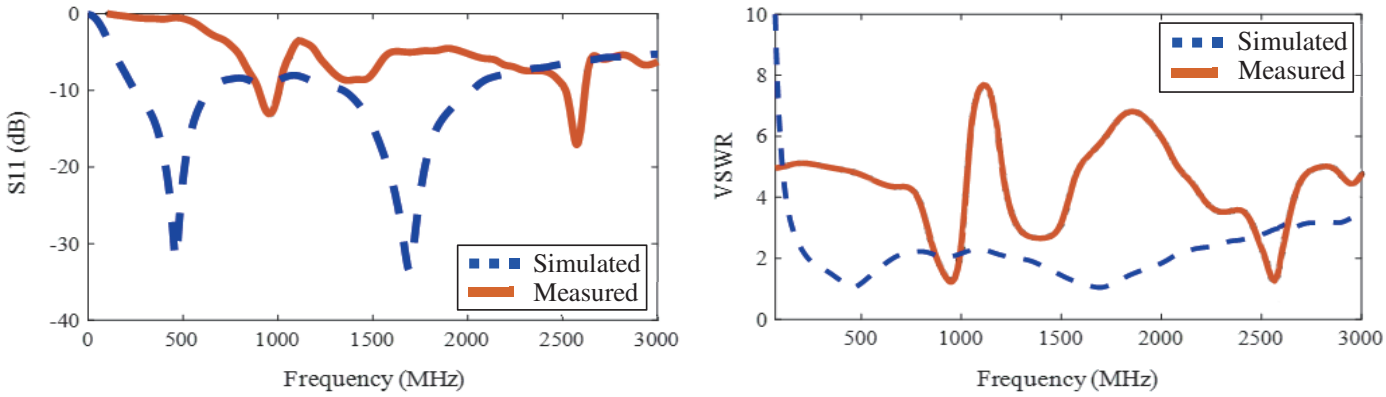

(a) (b)

FIGURE 7. Measured and simulated (a) S_{11}, and (b) VSWR.

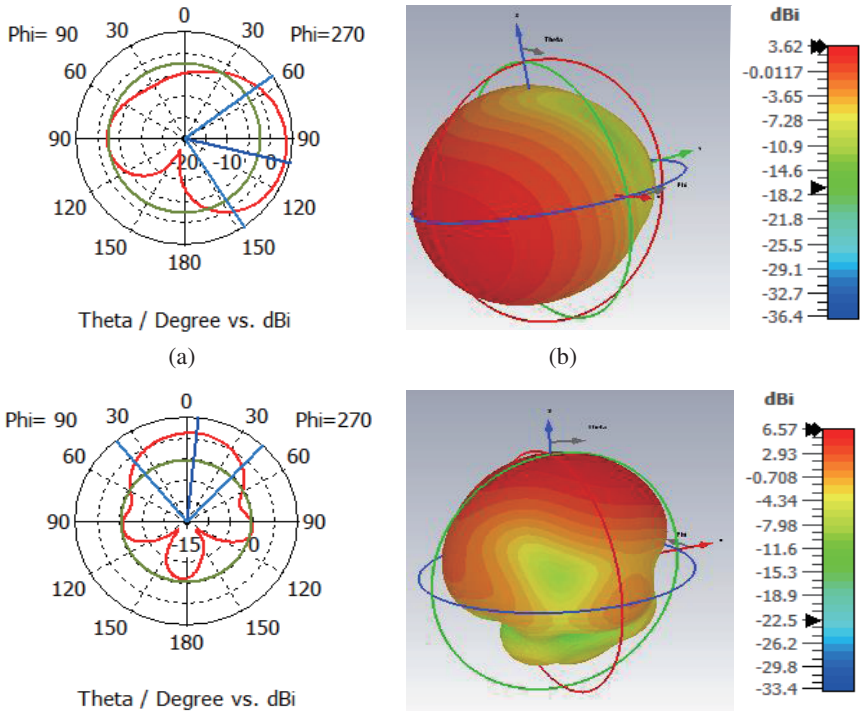

(a) (b)

(c) (d)

FIGURE 8. Radiation pattern of the antenna at 444 MHz in (a) 1D form and (b) 3D form, and at 1.65 GHz in (c) 1D form and (d) 3D form.

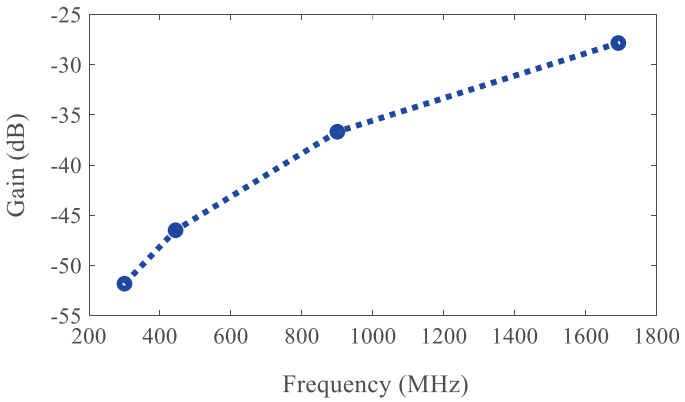

FIGURE 9. Realized gain of the proposed antenna.

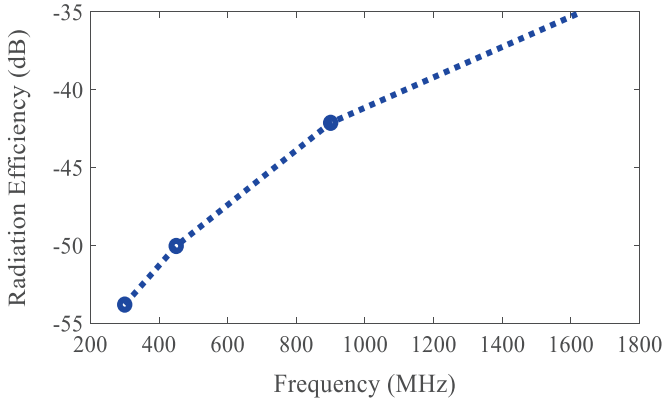

FIGURE 10. Radiation efficiency of the proposed antenna.

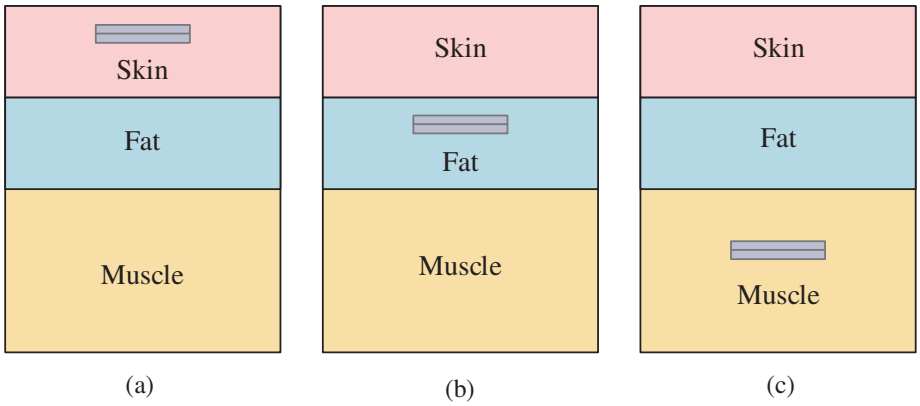

FIGURE 11. Antenna placement in different layers of human body phantom model.

erating frequency is near the MICS band, while the second is near the ISM band. Again, the VSWRs at the resonant frequencies are 1.073 and 1.031, respectively, indicating excellent impedance matching.

According to the measured results, the designed antenna presents two bands of 898.32–1003.5 MHz and 2.51–2.62 GHz, with resonance frequencies of 950.9 MHz and 2.58 GHz, respectively. So, the experimental results deviated from the simulated results. It occurred due to some manufacturing defects e.g., the shortening pin; superstrate could not be used, and pure FR-4 was not used as substrate, etc.

3.1.2. Radiation Pattern

Figure 8 depicts the radiation pattern of the proposed antenna obtained from simulation. The obtained main lobe magnitudes are 3.56 dB and 6.15 dB, having the direction along 103° and 6° at the resonant frequencies of 444 MHz and 1.65 GHz, respectively. Again, the side lobe levels are -5.9 dB and -6.3 dB at the resonant frequencies, respectively. Due to the unavailability of anechoic chamber, experimental results for radiation pattern and gain could not be obtained.

3.1.3. Gain

The realized gain in decibels of the proposed antenna is illustrated in Figure 9. The peak gains at the resonant frequencies are -46.5 dB and -28.2 dB at 444 MHz and 1.65 GHz, respectively.

3.1.4. Efficiency

The variation in radiation efficiency with respect to frequency of the proposed antenna is shown in Figure 10. At 444 MHz and 1.65 GHz, respectively, the radiation efficiencies are -50.3 dB and -34.78 dB.

3.2. Numerical Results in Human Body Phantom Model

To design an antenna suitable for wireless biotelemetry applications, it is essential to analyze the antenna's performance within the three layers of the human body environment. Therefore, a human body phantom model is constructed using CST software, incorporating human tissue properties outlined in Table 3. The antenna is subsequently positioned within various layers (skin, fat, and muscle) of this model, as shown in Figure 11.

3.2.1. Return Loss (S11 Parameter)

The return loss S_{11} of the proposed antenna within various layers of a human body phantom model is depicted in Figure 12. The S_{11} at the corresponding resonant frequencies are mentioned in Table 4.

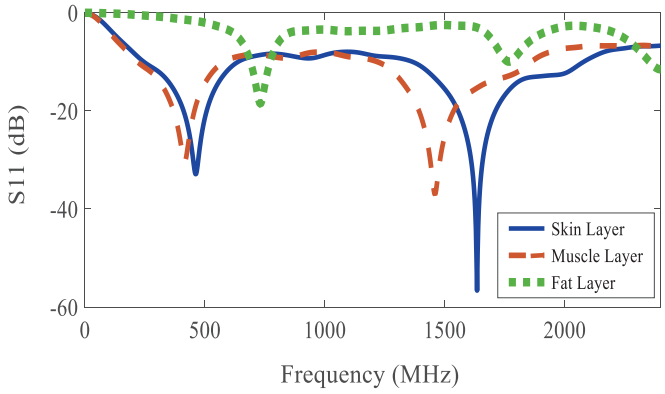

FIGURE 12. Return loss of the proposed antenna in the different layers of human body phantom model.

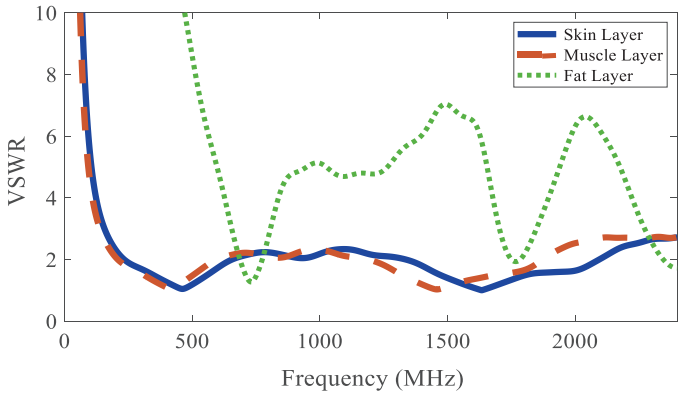

FIGURE 13. VSWR of the proposed antenna in the different layers of human body phantom model.

TABLE 3. Dielectric properties of tissue.

Biological Tissues	Dielctric Constant ϵ_r	Electrical Conductivity σ (S/m)
Skin	45.20	0.72
Fat	5.55	0.04
Muscle	56.60	0.82

TABLE 4. Return loss of the proposed antenna in different layers of human body phantom model.

Biological Tissue	Resonant Frequency (MHz)	Return Loss (dB)
Skin	464	−32.61
	1632	−58.96
Fat	729.7	−18.51
	1776.8	−9.79
Muscle	417.31	−30.59
	1473.44	−33.15

TABLE 5. VSWR of the proposed antenna in different layers of human body phantom model.

Biological Tissue	Resonant Frequency (MHz)	VSWR
Skin	464	1.049
	1632	1.019
Fat	729.7	1.27
	1776.8	1.93
Muscle	417.31	1.064
	1473.44	1.026

3.2.2. VSWR

The VSWRs of the proposed antenna within various layers of a human body phantom model are depicted in Figure 13. The VSWRs at the corresponding resonant frequencies are mentioned in Table 5. The results indicate sufficient impedance matching.

3.2.3. Gain

The realized gains of the proposed antenna within various layers of a human body phantom model are depicted in Figure 14. The magnitude of the obtained gains at the corresponding resonant frequencies are mentioned in Table 6. The results demonstrate sufficient gain for wireless transmission.

3.2.4. Directivity

The directivities of the proposed antenna within various layers of a human body phantom model are depicted in Figure 15. The magnitude of the obtained directivities at the corresponding resonant frequencies are mentioned in Table 7. The results demonstrate sufficient amount of directivity for wireless transmission.

3.2.5. Efficiency

The radiation efficiencies of the proposed antenna within various layers of a human body phantom model are depicted in Figure 16. The efficiencies at the corresponding resonant frequencies are mentioned in Table 8.

3.2.6. Specific Absorption Rate (SAR)

For safety concerns of the human body, SAR values are evaluated for implantation in different layers of the human body phantom model. Simulations are conducted under an input power of 0.5 W, yielding results based on the 1 g standard, as outlined in Table 9. Figures 17(a)–(b) illustrate the SAR distribution on the human body phantom model.

TABLE 6. Realized gain of the proposed antenna in different layers of human body phantom model.

Biological Tissue	Resonant Frequency (MHz)	Gain (dB)
Skin	464	−43.6
	1632	−24.5
Fat	729.7	−45.2
	1776.8	−24.6
Muscle	417.31	−43.9
	1473.44	−24.7

TABLE 7. Directivity of the proposed antenna in different layers of human body phantom model.

Biological Tissue	Resonant Frequency (MHz)	Directivity (dB)
Skin	464	1.68
	1632	3.39
Fat	729.7	5.67
	1776.8	2.27
Muscle	417.31	0.09
	1473.44	2.84

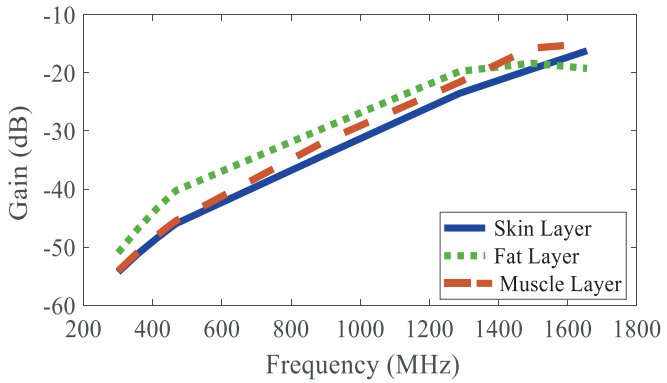

FIGURE 14. Realized gain of the proposed antenna in the different layers of human body phantom model.

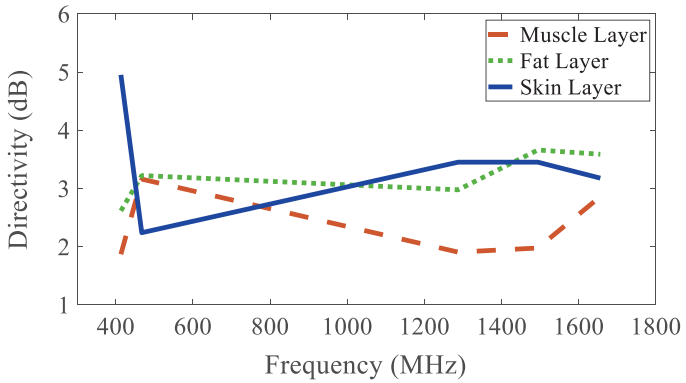

FIGURE 15. Directivity of the proposed antenna in the different layers of human body phantom model.

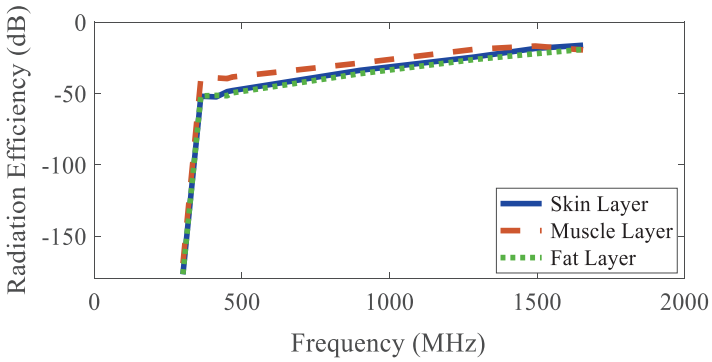

FIGURE 16. Radiation efficiency of the proposed antenna in the different layers of human body phantom model.

TABLE 8. Radiation efficiency of the proposed antenna in different layers of human body phantom model.

Biological Tissue	Resonant Frequency (MHz)	Radiation Efficiency (dB)
Skin	464	−49.57
	1632	−19.08
Fat	729.7	−51.36
	1776.8	−22.14
Muscle	417.31	−51.73
	1473.44	−26.22

TABLE 9. SAR values in different layers of human body model.

Biological Tissue	Resonant Frequency (MHz)	Maximum SAR (W/kg)
Skin	464	0.0489
	1632	1.1956
Fat	729.7	0.0410
	1776.8	1.1739
Muscle	417.31	0.00301
	1473.44	1.4

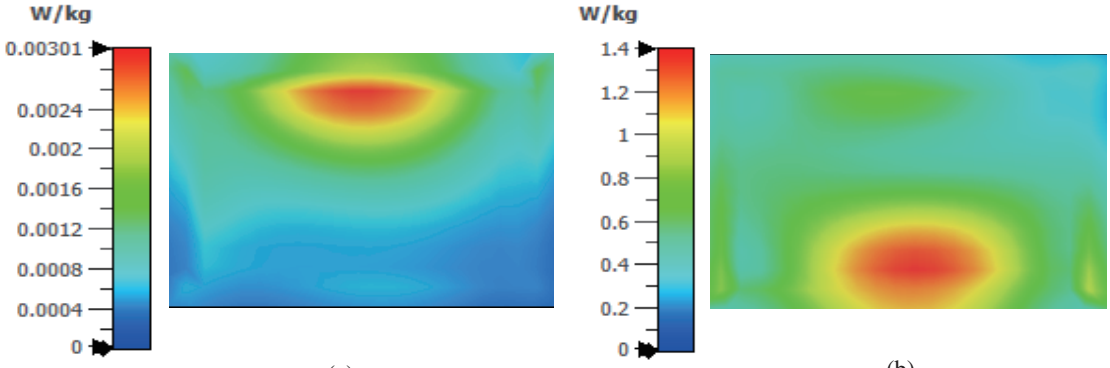

(a) (b)

FIGURE 17. SAR distribution of proposed antenna in the muscle layer at (a) 417.31 MHz and (b) 1473.44 MHz.

TABLE 10. Comparative analysis of the proposed antenna model with the existing antenna models.

Ref	Size (mm^3)	Antenna Type	Resonant Frequency (MHz)	Bandwidth (MHz)	Gain (dB)
[26]	17.92	Cavity Slot	2450	670	−26.5
[27]	28.85	Spiral Patch	915	915	−28
[28]	57.3	Fractal	403	92	−28.1
			2440	320	−31.3
[29]	3375	Cubic	2450	900	−18.5
			5800	1500	
[30]	71.43	Patch	2450	680	−32.8
[31]	15.87	Patch	1400	300	−27.6
			2450	380	−27.1
This Work	480	Spiral Patch with Slots	444	400	−46.5
			1655	887.9	−28.2

4. COMPARISON WITH THE EXISTING ANTENNAS

This paper proposes a spiral patch antenna which is loaded with patch slots and incorporates shortening pin which helps in improving return loss and increasing bandwidth. The previous studies adopted different techniques such as spiral patch (without slotting), fractal structure, cubic structure, and defective ground slots, which have their own advantages. Table 10 represents the comparative analysis of the proposed antenna geometry with the antennas reported in previous studies.

According to the comparative analysis shown in Table 10, the proposed antenna provides higher bandwidths than other antennas with sufficient gain. Though the antenna proposed in [29] has higher bandwidths, the proposed antenna is more compact. Again, the proposed design incorporates both the patch slots and shortening pin with coaxial feeding in spiral patch, which has not been utilized yet in previous studies. This combination helps in improving the impedance matching by providing smaller return losses. Moreover, the proposed design is less complicated than the other antenna designs.

5. CONCLUSION

A coaxial probe fed spiral shaped dual-band antenna for wireless biotelemetry applications is introduced in this work. The proposed antenna is designed to operate at 444 MHz (near the MICS band) and 1.65 GHz (near the ISM band). The obtained bandwidths are 400 MHz and 887.9 MHz, respectively. The proposed antenna is constructed on an FR-4 substrate. It consists of two symmetrical spiral elements, providing a total size of $27 \times 14 \times 1.6\,\text{mm}^3$. The coaxial probe feeding technique is used to excite the antenna. Low power losses due to reflection are achieved by the improved return losses, which are -46.5 dB and -28.2 dB at the respective resonant frequencies. Patch slots and shortening pins are incorporated in the antenna structure to improve its return loss and increase the bandwidths, representing a significant contribution to the field of dual-band antenna design for biotelemetry applications. The suggested antenna's experimental prototype is made on an FR-4 substrate. The experimental results demonstrate acceptable return loss and VSWR. Furthermore, within the human body phantom model, the obtained return losses are -32.61 dB and -58.96 dB at their respective resonant frequencies when the antenna is placed in the skin layer. Correspondingly, the gain values at these resonant frequencies are -46.5 dB and -28.2 dB. In the end, the SAR values of 48.9 mW/kg and 1.19 W/kg are obtained, meeting the safety requirements.

REFERENCES

[1] Gubbi, J., R. Buyya, S. Marusic, and M. Palaniswami, "Internet of Things (IoT): A vision, architectural elements, and future directions," *Future Generation Computer Systems*, Vol. 29, No. 7, 1645–1660, Sep. 2013.

[2] Das, R. and H. Yoo, "Biotelemetry and wireless powering for leadless pacemaker systems," *IEEE Microwave and Wireless Components Letters*, Vol. 25, No. 4, 262–264, Apr. 2015.

[3] Nikita, K. S., *Handbook of Biomedical Telemetry*, John Wiley & Sons, 2014.

[4] Chen, Y.-S., "Reduction of detuning effects using robust parameter design for implantable antennas," *Electronics Letters*, Vol. 51, No. 24, 1971–1973, Nov. 2015.

[5] Ung, J. and T. Karacolak, "A wideband implantable antenna for continuous health monitoring in the medradio and ism bands," *IEEE Antennas and Wireless Propagation Letters*, Vol. 11, 1642–1645, 2012.

[6] Islam, M. S., K. P. Esselle, D. Bull, and P. M. Pilowsky, "Converting a wireless biotelemetry system to an implantable system through antenna redesign," *IEEE Transactions on Microwave Theory and Techniques*, Vol. 62, No. 9, 1890–1897, Sep. 2014.

[7] Asif, S. M., J. Hansen, M. S. Khan, S. D. Walden, M. O. Jensen, B. D. Braaten, and D. L. Ewert, "Design and in vivo test of a batteryless and fully wireless implantable asynchronous pacing system," *IEEE Transactions on Biomedical Engineering*, Vol. 63, No. 5, 1070–1081, May 2016.

[8] Karacolak, T., A. Z. Hood, and E. Topsakal, "Design of a dual-band implantable antenna and development of skin mimicking gels for continuous glucose monitoring," *IEEE Transactions on Microwave Theory and Techniques*, Vol. 56, No. 4, 1001–1008, Apr. 2008.

[9] Shah, S. A. A. and H. Yoo, "Scalp-implantable antenna systems for intracranial pressure monitoring," *IEEE Transactions on Antennas and Propagation*, Vol. 66, No. 4, 2170–2173, Apr. 2018.

[10] Gani, I. and H. Yoo, "Multi-band antenna system for skin implant," *IEEE Microwave and Wireless Components Letters*, Vol. 26, No. 4, 294–296, 2016.

[11] Das, R. and H. Yoo, "A wideband circularly polarized conformal endoscopic antenna system for high-speed data transfer," *IEEE Transactions on Antennas and Propagation*, Vol. 65, No. 6, 2816–2826, Jun. 2017.

[12] Yun, S., K. Kim, and S. Nam, "Outer-wall loop antenna for ultra-wideband capsule endoscope system," *IEEE Antennas and Wireless Propagation Letters*, Vol. 9, 1135–1138, 2010.

[13] Soora, S., K. Gosalia, M. S. Humayun, and G. Lazzi, "A comparison of two and three dimensional dipole antennas for an implantable retinal prosthesis," *IEEE Transactions on Antennas and Propagation*, Vol. 56, No. 3, 622–629, Mar. 2008.

[14] Zaki, A. Z. A., E. K. I. Hamad, T. G. Abouelnaga, H. A. Elsadek, S. A. Khaleel, A. J. A. Al-Gburi, and Z. Zakaria, "Design and modeling of ultra-compact wideband implantable antenna for wireless ISM band," *Bioengineering*, Vol. 10, No. 2, 216, Feb. 2023.

[15] Padhi, S. K., N. C. Karmakar, C. L. Law, and S. Aditya, "A dual polarized aperture coupled circular patch antenna using a C-shaped coupling slot," *IEEE Transactions on Antennas and Propagation*, Vol. 51, No. 12, 3295–3298, 2003.

[16] Liu, W.-C., C.-M. Wu, and Y. Dai, "Design of triple-frequency microstrip-fed monopole antenna using defected ground structure," *IEEE Transactions on Antennas and Propagation*, Vol. 59, No. 7, 2457–2463, Jul. 2011.

[17] Arif, A., M. Zubair, M. Ali, M. U. Khan, and M. Q. Mehmood, "A compact, low-profile fractal antenna for wearable on-body WBAN applications," *IEEE Antennas and Wireless Propagation Letters*, Vol. 18, No. 5, 981–985, May 2019.

[18] Duan, Z., Y.-X. Guo, R.-F. Xue, M. Je, and D.-L. Kwong, "Differentially fed dual-band implantable antenna for biomedical applications," *IEEE Transactions on Antennas and Propagation*, Vol. 60, No. 12, 5587–5595, Dec. 2012.

[19] Soontornpipit, P., C. M. Furse, and Y. C. Chung, "Design of implantable microstrip antenna for communication with medical implants," *IEEE Transactions on Microwave Theory and Techniques*, Vol. 52, No. 8, 1944–1951, Aug. 2004.

[20] Islam, M. S., K. P. Esselle, D. Bull, and P. M. Pilowsky, "Converting a wireless biotelemetry system to an implantable system through antenna redesign," *IEEE Transactions on Microwave Theory and Techniques*, Vol. 62, No. 9, 1890–1897, Sep. 2014.

[21] Huang, F.-J., C.-M. Lee, C.-L. Chang, L.-K. Chen, T.-C. Yo, and C.-H. Luo, "Rectenna application of miniaturized implantable antenna design for triple-band biotelemetry communication," *IEEE Transactions on Antennas and Propagation*, Vol. 59, No. 7, 2646–2653, Jul. 2011.

[22] Kaim, V., B. K. Kanaujia, S. Kumar, H. C. Choi, K. W. Kim, and K. Rambabu, "Ultra-miniature circularly polarized CPW-fed implantable antenna design and its validation for biotelemetry applications," *Scientific Reports*, Vol. 10, No. 1, 6795, Apr. 2020.

[23] Dayo, Z. A., M. Aamir, S. A. Dayo, I. A. Khoso, P. Soothar, F. Sahito, T. Zheng, Z. Hu, and Y. Guan, "A novel compact broadband and radiation efficient antenna design for medical iot healthcare system," *Mathematical Biosciences and Engineering*, Vol. 19, No. 4, 3909–3927, 2022.

[24] Zaki, A. Z. A., E. K. I. Hamad, T. G. Abouelnaga, H. A. Elsadek, S. A. Khaleel, A. J. A. Al-Gburi, and Z. Zakaria, "Design and modeling of ultra-compact wideband implantable antenna for wireless ism band," *Bioengineering*, Vol. 10, No. 2, 216, Feb. 2023.

[25] Huang, Z., H. Wu, S. S. Mahmoud, and Q. Fang, "Design of a novel compact MICS band PIFA antenna for implantable biotelemetry applications," *Sensors*, Vol. 22, No. 21, 8182, 2022.

[26] Palandoken, M., "Compact bioimplantable MICS and ISM band antenna design for wireless biotelemetry applications," *Radioengineering*, Vol. 26, No. 4, 917–923, Dec. 2017.

[27] Xia, W., K. Saito, M. Takahashi, and K. Ito, "Performances of an implanted cavity slot antenna embedded in the human arm," *IEEE Transactions on Antennas and Propagation*, Vol. 57, No. 4, 894–899, Apr. 2009.

[28] Basir, A. and H. Yoo, "A stable impedance-matched ultrawideband antenna system mitigating detuning effects for multiple biotelemetric applications," *IEEE Transactions on Antennas and Propagation*, Vol. 67, No. 5, 3416–3421, May 2019.

[29] Fan, Y., H. Liu, X. Liu, Y. Cao, Z. Li, and M. M. Tentzeris, "Novel coated differentially fed dual-band fractal antenna for implantable medical devices," *IET Microwaves, Antennas & Propagation*, Vol. 14, No. 2, 199–208, 2020.

[30] Kaim, V., B. K. Kanaujia, and K. Rambabu, "Quadrilateral spatial diversity circularly polarized MIMO cubic implantable antenna system for biotelemetry," *IEEE Transactions on Antennas and Propagation*, Vol. 69, No. 3, 1260–1272, Mar. 2021.

[31] Xu, C., Y. Fan, and X. Liu, "A circularly polarized implantable rectenna for microwave wireless power transfer," *Micromachines*, Vol. 13, No. 1, 121, Jan. 2022.

[32] Zhang, J., R. Das, D. Hoare, H. Wang, A. Ofiare, N. Mirzai, J. Mercer, and H. Heidari, "A compact dual-band implantable antenna for wireless biotelemetry in arteriovenous grafts," *IEEE Transactions on Antennas and Propagation*, Vol. 71, No. 6, 4759–4771, Jun. 2023.

[33] Liu, C., Y.-X. Guo, and S. Xiao, "Circularly polarized helical antenna for ISM-band ingestible capsule endoscope systems," *IEEE Transactions on Antennas and Propagation*, Vol. 62, No. 12, 6027–6039, Dec. 2014.

[34] Li, H., Y.-X. Guo, C. Liu, S. Xiao, and L. Li, "A miniature-implantable antenna for medradio-band biomedical telemetry," *IEEE Antennas and Wireless Propagation Letters*, Vol. 14, 1176–1179, 2015.

[35] Shah, S. A. A. and H. Yoo, "Scalp-implantable antenna systems for intracranial pressure monitoring," *IEEE Transactions on Antennas and Propagation*, Vol. 66, No. 4, 2170–2173, Apr. 2018.

[36] Ma, S., T. Bjorninen, L. Sydanheimo, M. H. Voutilainen, and L. Ukkonen, "Double split rings as extremely small and tuneable antennas for brain implantable wireless medical microsystems," *IEEE Transactions on Antennas and Propagation*, Vol. 69, No. 2, 760–768, Feb. 2021.

[37] Han, L., W. Zhang, X. Chen, G. Han, and R. Ma, "Design of compact differential dual-frequency antenna with stacked patches," *IEEE Transactions on Antennas and Propagation*, Vol. 58, No. 4, 1387–1392, Apr. 2010.